Dynamical causes for incipient magma chambers above slabs

Taras V. Gerya* Institute of Geology, Mineralogy, and Geophysics, Ruhr-University Bochum, 44780 Bochum, Germany, and Institute of Experimental Mineralogy, Russian Academy of Sciences, 142432 Chernogolovka, Moscow, Russia

David A. Yuen, Erik O.D. Sevre University of Minnesota Supercomputing Institute and Department of Geology and Geophysics, University of Minnesota, Minneapolis, Minnesota 55455-0219, USA

ABSTRACT

Using a regional upper-mantle model with an unprecedented spatial resolution of ~100 m, we have investigated at multiple resolutions the character of incipient magma chambers forming under oceanic arcs. The magma chambers are formed from wave-like structures propagating upward along descending slabs and consist of compositionally buoyant, hydrated, partially molten subducted crustal and mantle material. These wave structures are 300–500 °C colder than the mantle wedge and may have an upward velocity of >1 m/yr. Inverted temperature structures and transitory bimodal magmatism are plausible consequences of finger-like penetration of relatively cold, hydrated material of the incipient magma chambers into the hot mantle wedge. Apart from forming and periodic feeding of the magma chambers, "cold" waves may also transport upward thousands of cubic kilometers of subducted material and may cause the rapid exhumation of ultrahigh-pressure rocks along slabs.

Keywords: subduction zones, numerical modeling, partial melting, mantle plumes, exhumation of ultrahigh-pressure rocks.

INTRODUCTION

Diapiric flows or upwellings in the mantle are propelled by either thermal or chemical buoyancy and have various morphologies (Hansen and Yuen, 1988; Bercovici and Mahoney, 1994; Cserepes and Yuen, 2000). Another plausible mechanism of mass transport in the mantle involves porous melt or fluid flows (Davies and Stevenson, 1992; Stern, 2002). Similar features are also expected to develop under volcanic arcs, because of hydration and melting on the top of the subducting slabs (Marsh, 1979; Davies and Stevenson, 1992; Tamura et al., 2002; Hall and Kincaid, 2001; Stern, 2002). Some geodynamic and volcanologic aspects of the hydration, partial melting, and mantle circulation atop subducting slabs have already been addressed by numerical (Davies and Stevenson, 1992; Gerya and Yuen, 2003a) and laboratory (Hall and Kincaid, 2001) experiments. However, up to now, there has been no coupled thermal-chemical-mechanical-rheological model of an incipient magma chamber accounting for the combined effects of both hydration and partial melting (Marsh, 1979; Stern, 2002). We describe below a new ultrahigh-resolution two-dimensional numerical model that can reproduce these enigmatic features above subducting slabs.

NUMERICAL MODEL

We have designed a regional two-dimensional upper-mantle model (Fig. 1) with a kinematically prescribed subducting plate (Gerya and Yuen, 2003a). The boundary conditions correspond to the corner-flow model, which accounts for asthenospheric mantle flow under the overriding plate. The top surface is calculated dynamically like a free surface by using an 8-km-thick top layer with a lower viscosity (10^{16} Pa·s) and density (1 kg/m^3 for the atmosphere, 1000 kg/m^3 for the seawater).

In a situation where the availability of water controls the progress of the mantle hydration (e.g., Peacock, 1987), spatial changes in the hydration rate (v_h) along the hydration front (Fig. 1) should mainly depend on spatial changes in the rate of fluid release along the surface of the subducting plate (Kerrick and Connolly, 2001). Using a simplified linear dehydration model of the subducting slab (Gerya et al., 2002), we assume that the hydration rate can be roughly approximated as follows:

$$v_h = 0.07 v_s \quad \text{when } x < x_{lim},$$
$$v_h = 0 \quad \text{when } x > x_{lim}, \qquad (1)$$

where v_s is the subduction rate (m/s) and x_{lim} = 150 km is the limiting horizontal distance (x) from the trench to the right of which the fluid release from the subducting plate is negligible (Gerya et al., 2002).

We assume that partial melting occurs in the pressure-temperature (P-T) region between the wet solidus and the dry liquidus (Table 1), defined experimentally for three hydrated petrologic components: hydrated mantle, subducted sediments, and oceanic crust. As a first

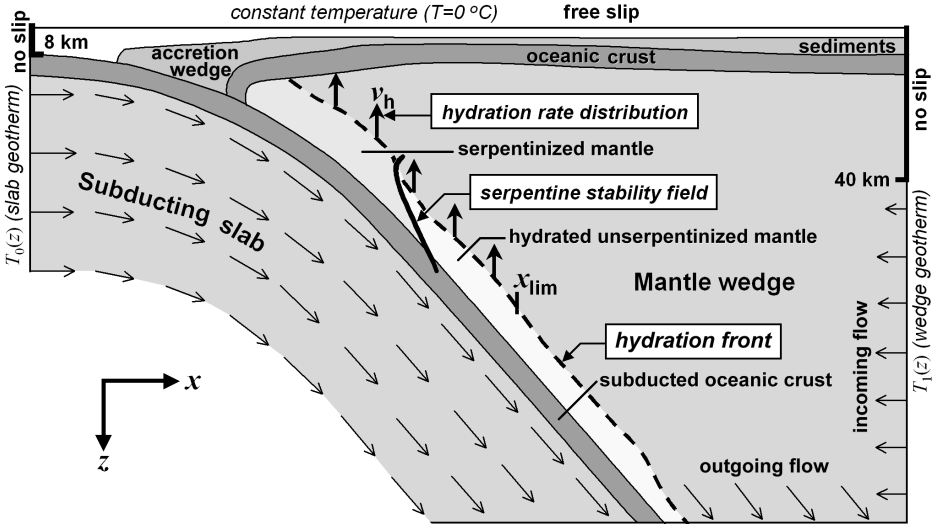

Figure 1. Numerical upper-mantle model designed for our two-dimensional numerical experiments. An intermediate stage of calculation with well-developed hydrated mantle zone is shown. Initial conditions for calculation (Gerya and Yuen, 2003a) are taken as follows: initial position of subduction zone is prescribed by weak, 8-km-thick, hydrated peridotite layer; initial temperature field in subducting plate is defined by an oceanic geotherm $T_0(z)$ with specified age; initial temperature distribution in overriding plate $T_1(z)$ corresponds to equilibrium thermal profile with 0 °C at surface and 1350 °C at 32 km depth; initial structure of 8-km-thick oceanic crust is taken as follows (from top to bottom): sedimentary rocks = 1 km, basaltic layer = 2 km, gabbroic layer = 5 km. Serpentine stability field (Table 1) is taken according to the experimental data for antigorite (Schmidt and Poli, 1998). Further details of model design and limitations are given by Gerya and Yuen (2003a).

*E-mail: taras.gerya@ruhr-uni-bochum.de.

TABLE 1. MATERIAL PROPERTIES USED IN TWO-DIMENSIONAL NUMERICAL EXPERIMENTS

Material	ρ_0 (kg/m^3)	Thermal conductivity [W/(m·K)]	Rheology	$T_{solidus}$ (K)	$T_{liquidus}$ (K)	H_L (kJ/kg)
Sedimentary rocks	2700 (solid)	$0.64 + 807/(T + 77)$	constant viscosity	$889 + 17900/(P + 54) + 20200/(P + 54)^2$ at $P < 1200$ MPa,	$1262 + 0.09P$	300
	2400 (molten)		10^{19} Pa·s	$831 + 0.06P$ at $P > 1200$ MPa		
Basaltic crust	3100 (solid)	$1.18 + 474/(T + 77)$	constant viscosity	$973 - 70400/(P + 354) + 77800000/(P + 354)^2$ at $P < 1600$ MPa,	$1423 + 0.105P$	380
	2900 (molten)		10^{19} Pa·s	$935 + 0.0035P + 0.0000062P^2$ at $P > 1600$ MPa		
Gabbroic crust	3100 (solid)	$1.18 + 474/(T + 77)$	plagioclase (An75)	$973 - 70400/(P + 354) + 77800000/(P + 354)^2$ at $P < 1600$ MPa,	$1423 + 0.105P$	380
	2900 (molten)		flow law	$935 + 0.0035P + 0.0000062P^2$ at $P > 1600$ MPa		
Serpentinized mantle	3000	$0.73 + 1293/(T + 77)$	constant viscosity 10^{19} Pa·s	–	–	–
Hydrated unserpentinized mantle*	3200 (solid)	$0.73 + 1293/(T + 77)$	wet olivine	$1240 + 49800/(P + 323)$ at $P < 2400$ MPa,	$2073 + 0.114P$	300
	3000 (molten)		flow law	$1266 - 0.0118P + 0.0000035P^2$ at $P > 2400$ MPa		
Dry mantle	3300	$0.73 + 1293/(T + 77)$	dry olivine flow law	–	–	–
References	(Turcotte and Schubert, 1982)	(Clauser and Huenges, 1995)	(Gerya et al., 2002; Ranalli, 1995)	(Schmidt and Poli, 1998; Poli and Schmidt, 2002)	(Schmidt and Poli, 1998; Poli and Schmidt, 2002)	(Turcotte and Schubert, 1982; Bittner and Schmeling, 1995)

Note: reference model parameters (Fig. 2): box size—400 km × 200 km; grid resolution—401 × 201 regularly spaced points, ~12 × 10^6 markers randomly distributed; subducting lithosphere age 80 m.y.; subduction rate v_s = 2 cm/yr; lateral viscosity variation 10^{16}–10^{26} Pa·s.

*Hydrated mantle beyond the antigorite stability field (Schmidt and Poli, 1998): $T > 751 + 0.18P - 0.000031P^2$ at $P < 2100$ MPa, $T > 1013 - 0.0018P - 0.0000039P^2$ at $P > 2100$ MPa.

approximation, the volumetric degree of melting M is taken to increase linearly with the temperature:

$$M = \begin{cases} 0 & \text{at } T < T_{solidus} \\ \dfrac{T - T_{solidus}}{T_{liquidus} - T_{solidus}} & \text{at } T_{solidus} < T < T_{liquidus} \\ 1 & \text{at } T > T_{liquidus}, \end{cases} \quad (2)$$

where $T_{solidus}$ and $T_{liquidus}$ are, respectively, wet solidus temperature and dry liquidus temperature at a given pressure and rock composition (Table 1). An effective density (ρ_{eff}) of partially molten rocks is calculated as

$$\rho_{eff} = \rho_{solid} - M(\rho_{solid} - \rho_{molten}), \quad (3)$$

where ρ_{solid} and ρ_{molten} are, respectively, densities of solid and molten rock. Effective heat capacity of partially molten rocks is expressed as

$$C_{p,eff} = C_p + H_L/(T_{liquidus} - T_{solidus}), \quad (4)$$

where C_p = 1000 J/(K·kg) is the heat capacity of solid rocks and H_L is latent heat of melting (Table 1).

The effective creep viscosity of solid rocks ($M < 0.1$), depending on the stress and temperature, is represented by experimentally determined flow laws (Table 1). The effective viscosity of molten rocks ($M > 0.1$) is calculated as (Pinkerton and Stevenson, 1992)

$$\eta = \eta_o \exp\{2.5 + [(1 - M)/M]^{0.48} \times (1 - M)\}, \quad (5)$$

where $\eta_o = 10^{13}$ Pa·s is taken for the basic oceanic crust and hydrated peridotite and $\eta_o = 5 \times 10^{14}$ Pa·s is used for the felsic sedimentary rocks (Bittner and Schmeling, 1995).

We have solved the momentum, continuity, and temperature equations within the framework of the two-dimensional creeping-flow approximation and have considered both thermal and chemical buoyancies along with mechanical heating from adiabatic work and viscous dissipation. We have employed the code I2VIS (Gerya and Yuen, 2003b), which is based on finite differences with a nondiffusive-marker-in-cell technique. Altogether we have carried out ~50 high-resolution numerical runs with various subduction rates (2–10 cm/yr) and slab ages (40–130 m.y.) on a 401 × 201 regular Eulerian grid with ~12 × 10^6 markers for the chemical components, the temperature field, and other transport properties represented. This algorithm allows us to resolve fine details with an unprecedented spatial accuracy of ~100 m, which is necessary to capture incipient magma chambers.

RESULTS OF SIMULATION

Figures 2 and 3 summarize the results of our reference model (Table 1). Further details for this model and related numerical experiments are available at http://www.msi.umn.edu/~esevre/people/taras/, or http://tomo.msi.umn.edu/~max/webis/. The initial stages, younger than 10 m.y., are characterized by the progressive hydration of the mantle wedge, resulting in the propagation upward of a sharp hydration front from the subducting slab. The hydrated mantle is subdivided into two parts: an upper, serpentinized, subduction channel developing within an upper, colder, lithospheric part ($T < 1000$ °C) of the wedge, and a lower, hydrated, but not serpentinized, peridotite zone developing within a lower, hotter, asthenospheric part ($T > 1000$ °C) outside of the *P-T* stability field of serpentine (Fig. 1, Table 1). These two zones are separated by the zone of narrowing (Figs. 2 and 3) caused by the forced flow of the asthenospheric mantle toward the subducting plate. The narrowing also produces a wedge-shaped closure of the serpentinized subduction channel, forcing a backward flow (Gerya et al., 2002) within the channel (Figs. 2 and 3).

Afterward, 10–17 m.y. later, there emerges a wave-like Rayleigh-Taylor instability (Ramberg, 1981) along the upper surface of the serpentine-free hydrated peridotite zone. This buoyancy-driven instability is caused by the strong (100–200 kg/m^3) density contrast (Hall and Kincaid, 2001) between the hydrated, lower-density peridotite mixed with partially molten subducted oceanic crust and the higher-density, overriding dry asthenosphere. On the other hand, the effective dynamic viscosity of the hydrated mantle wedge (10^{17}–10^{19} Pa·s) is several orders of magnitude lower (Fig. 2, right column) than either the effective dynamic viscosity of the cold sub-

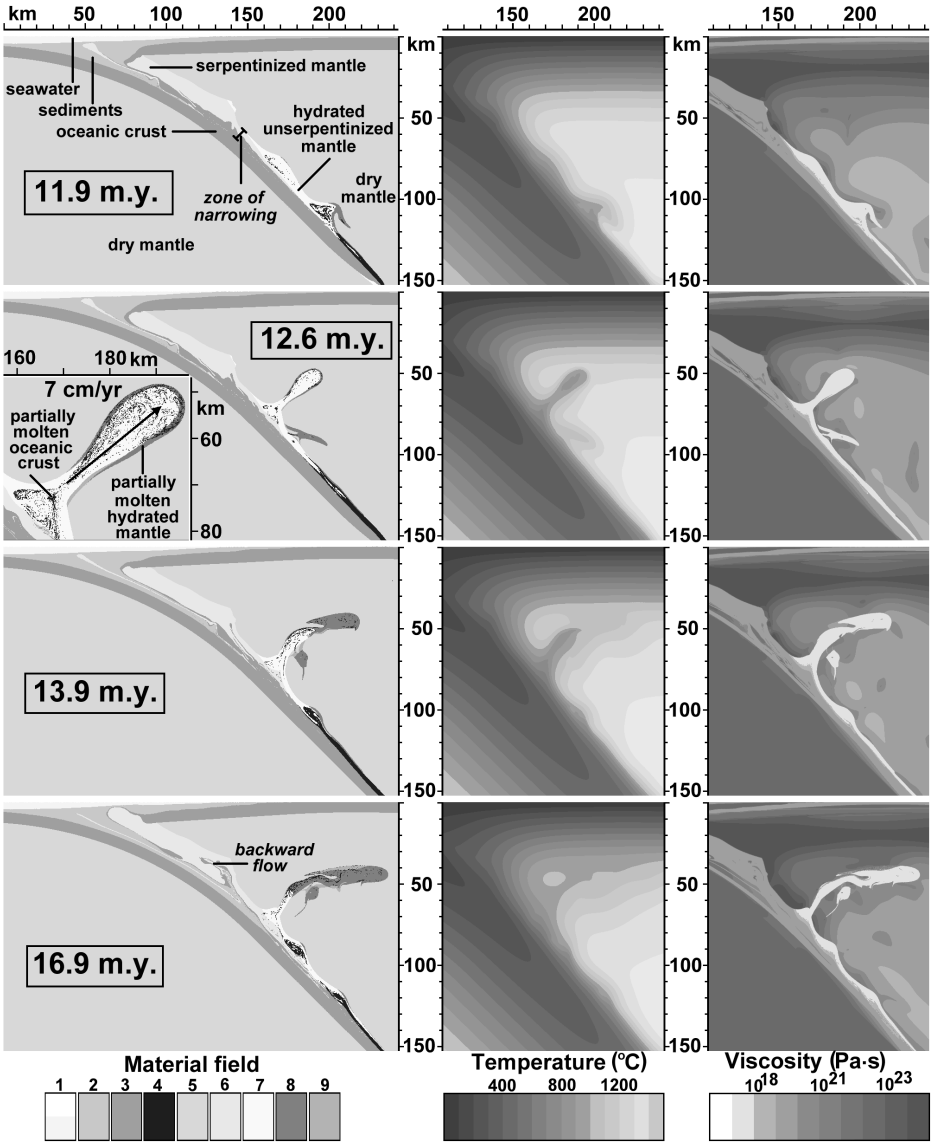

Figure 2. Dynamics of development of incipient magma chamber under oceanic arc during early (12–17 m.y.) stages of ongoing subduction. Three columns show temporal evolution of material field (left column), temperature distribution (middle column), and viscosity field (right column) of mantle wedge. Sketches represent 240 km × 150 km areas of original 400 km × 200 km model. Left: Evolution of distribution of rock types shading: 1—weak layer on top of model (air, seawater); 2—sedimentary rocks; 3 and 4—solid and partially molten oceanic crust, respectively; 5—dry mantle; 6—serpentinized mantle; 7—hydrated unserpentinized mantle; 8—partially molten hydrated mantle; 9—mantle quenched after partial melting. Close-up area reveals details of initial (finger-like) stage of propagation of incipient magma chamber into hot mantle wedge; arrow shows direction of motion for this structure.

ducting slab ($>10^{20}$ Pa·s) or that of the overriding dry mantle (10^{19}–10^{22} Pa·s). Therefore, favorable conditions are created for the rapid escape of buoyant wave-like features upward along the subducting plate within the hydrated and partially molten, low-viscosity hydrated peridotite zone (Fig. 2, right column).

The shape and the internal geometry of the wave-like structures are very complex (Fig. 2, 11.9 m.y.), reflecting the internal deformation and rotation of rocks within these waves (Fig. 3). This shape results from an interaction of several competing processes: (1) subduction of material along the bottom of a wave, (2) deformation of the dry mantle atop the wave, (3) growth of the wave amplitude, which tends to produce diapiric structures (Ramberg, 1981), and (4) upward propagating escape of the wave, which tends to preserve its shape within the low viscosity zone, which is analogous to solitary waves (Olson and Christensen, 1986).

The upward velocity of the waves often exceed the subduction speed (Fig. 3). In the reference model shown in Figures 2 and 3, the wave velocity varies from 0.3–25 cm/yr; in other numerical experiments, this velocity reaches >1 m/yr. Apart from strong density contrast between the dry mantle and hydrated, partially molten rocks composing waves, this high velocity is controlled by the low effective viscosity (10^{19}–10^{21} Pa·s) of the dry mantle deforming atop the waves (Fig. 2, right column).

Merging of several wave-like structures rising with different velocities (Fig. 3A) commonly occurs and may cause the growth of rapidly propagating diapiric and finger-like structures at a shallower level (Fig. 2, 12.6 m.y.), giving rise to the formation of an incipient magma chamber. The inverted temperature gradient within the source area of the diapir at the subducting slab results in an intriguing geologic phenomenon: the hydrated, partially molten, finger-like structure rising through the mantle wedge is 300–500 °C colder than the surrounding wedge material (Tamura, 1994; Gerya and Yuen, 2003a). Increase in temperature in the outer zones of this rising ''cold'' plume results from both shear heating and thermal interaction with the hot mantle wedge (Gerya and Yuen, 2003a). As suggested by Tamura (1994), this may form favorable conditions for transitory bimodal magmatism because of both the compositional and the thermal zoning of the incipient magma chamber (Fig. 2, 12.6 m.y.), which would generate basalts from its water-depleted, hot rind, and boninites from its water-enriched, cooler interior. Further massive heating of this structure from the wedge eliminates thermal zoning and causes underplating of the lithospheric mantle below the volcanic arc by the flattened (30–50 km wide and 5–15 km thick) magma chamber composed of hydrated, partially molten material (Fig. 2, 13.9 m.y., 16.9 m.y.) connected with the hydrated, planar subduction channel by the radial conduit (Figs. 3B and 3C). The newly discovered partially molten wave-like structures (''cold'' waves) ascending along the slab may penetrate through the radial conduit and periodically feed the magma chamber (Fig. 3B). This rapid penetration may cause a new period of bimodal magmatism owing to the renewal of thermal and compositional zoning within the magma chamber (Fig. 2, 13.9 m.y., Fig. 3B). The physical nature of ''cold'' waves rising through the radial conduit is apparently similar to ''hot'' solitary waves propagating outward in a radial magmatic channel (Olson and Christensen, 1986).

The ''cold'' waves represent a very efficient, rapid, upward-transport media. In contrast to finger-like and diapiric structures penetrating the relatively hot mantle wedge, the ''cold'' waves rising along the slab interface are not subjected to the strong heating from the wedge mantle and are characterized by a relatively stable temperature varying between 800 and 1100 °C. Therefore, similar waves can transport thousands of cubic kilometers (Fig. 3) of previously subducted, relatively

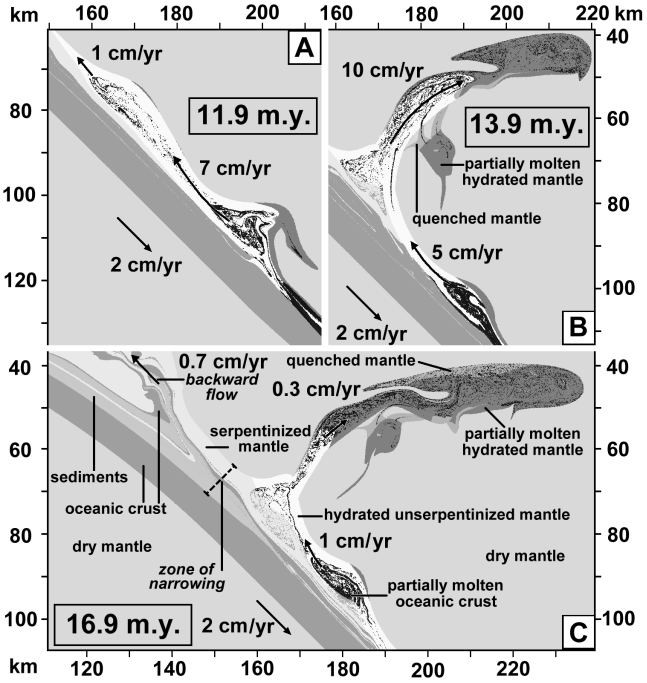

Figure 3. Close-up view of incipient magma chamber and selected wave-like structures developed in numerical simulations. See left column of Figure 2 for location of these structures and shading code. Arrows show direction of propagation of "cold" waves.

cold, but chemically buoyant material upward from depths of >100 km toward the bottom of the serpentinized subduction channel, where further exhumation of this material due to the backward flow in the serpentinized channel (Fig. 3C) can occur (Gerya et al., 2002). Therefore, ''cold'' waves may explain the rapid exhumation of ultrahigh-pressure coesite- and diamond-bearing rocks of both crustal and mantle origin found in several orogenic belts and characterized by 750–1100 °C temperatures at peak metamorphism (Rosen et al., 1972; Chopin, 1984; Sobolev and Shatsky, 1990; Dobrzhinetskaya et al., 1996; Stöckhert et al., 2001).

DISCUSSION AND CONCLUSIONS

Rapid propagation of both small-scale (1–10 km) cold finger-like structures and cold waves moving upward may wield important control over the spatial distribution of volcanic and seismic activities in regions of subduction (Tamura, 1994; Hall and Kincaid, 2001; Gerya and Yuen, 2003a). Our results also appear to be realistic, when they are compared with the seismic data revealing the complexity of seismicity distributions at subduction zones, especially near the Japanese Trench (Zhao et al., 2002). Negative seismic velocity anomalies found in the Japanese arc constitute a particular feature that might be reinterpreted in light of our results. Rather than regarding them as thermal anomalies (Tamura et al., 2002), we interpret these low-seismic-velocity anomalies (Zhao et al., 2002) near Japan as indicating some traces of water (Jung and Karato, 2001). The generation and propagation of incipient magma chambers above slabs depends strongly on the dynamics imposed by the subduction rate and the thermal constraints posed by the age of the slab and the asthenospheric circulation above the slab (Davies and Stevenson, 1992; Gerya and Yuen, 2003a; Stern, 2002).

ACKNOWLEDGMENTS

This work was supported by Russsian Foundation of Basic Research grant no. 03-05-64633, by an Alexander von Humboldt Foundation Research Fellowship to Gerya, the geophysics program of the National Science Foundation, and by the German Science Foundation within SFB 526. Constructive reviews by J. Connolly and R.J. Stern are greatly appreciated.

REFERENCES CITED

Bercovici, D., and Mahoney, J., 1994, Double flood basalts and plume head separation at the 660-kilometer discontinuity: Science, v. 266, p. 1367–1369.

Bittner, D., and Schmeling, H., 1995, Numerical modeling of melting processes and induced diapirism in the lower crust: Geophysical Journal International, v. 123, p. 59–70.

Chopin, C., 1984, Coesite and pure pyrope in high-grade blueschists of the Western Alps: A first record and some consequences: Contributions to Mineralogy and Petrology, v. 86, p. 107–118.

Clauser, C., and Huenges, E., 1995, Thermal conductivity of rocks and minerals, *in* Ahrens, T.J., ed., Rock physics and phase relations: Washington, D.C., American Geophysical Union, Reference Shelf 3, p. 105–126.

Cserepes, L., and Yuen, D.A., 2000, On the possibility of a second kind of mantle plume: Earth and Planetary Science Letters, v. 183, p. 61–71.

Davies, H.J., and Stevenson, D.J., 1992, Physical model of source region of subduction zone volcanics: Journal of Geophysical Research, v. 97, p. 2037–2070.

Dobrzhinetskaya, L.F., Green, H.W., II, and Wang, S., 1996, Alpe Arami: A peridotite massif from depths of >300 km: Science, v. 271, p. 1841–1845.

Gerya, T.V., and Yuen, D.A., 2003a, Rayleigh-Taylor instabilities from hydration and melting propel ''cold plumes'' at subduction zones: Earth and Planetary Science Letters, v. 212, p. 47–62.

Gerya, T.V., and Yuen, D.A., 2003b, Characteristics-based marker-in-cell method with conservative finite-differences schemes for modeling geological flows with strongly variable transport properties: Physics of the Earth and Planetary Interiors (in press).

Gerya, T.V., Stoeckhert, B., and Perchuk, A.L., 2002, Exhumation of high-pressure metamorphic rocks in a subduction channel—A numerical simulation: Tectonics, v. 21, p. 6-1–6-19.

Hall, P.S., and Kincaid, C., 2001, Diapiric flow at subduction zones: A recipe for rapid transport: Science, v. 292, p. 2472–2475.

Hansen, U., and Yuen, D.A., 1988, Numerical simulations of thermal-chemical instabilities and lateral heterogeneities at the core-mantle boundary: Nature, v. 334, p. 237–240.

Jung, H., and Karato, S., 2001, Water-induced fabric transitions in olivine: Science, v. 293, p. 1460–1463.

Kerrick, D.M., and Connolly, J.A.D., 2001, Metamorphic devolatilization of subducted oceanic metabasalts: Implications for seismicity, arc magmatism and volatile recycling: Earth and Planetary Science Letters, v. 189, p. 19–29.

Marsh, B.D., 1979, Island-arc development: Some observation, experiments and speculations: Journal of Geology, v. 87, p. 687–713.

Olson, P., and Christensen, U., 1986, Solitary wave propagation in a fluid conduit within a viscose matrix: Journal of Geophysical Research, v. 91, p. 6367–6374.

Peacock, S.M., 1987, Serpentinization and infiltration metasomatism in the Trinity peridotite, Klamath province, northern California: Implications for subduction zones: Contributions to Mineralogy and Petrology, v. 95, p. 55–70.

Pinkerton, H., and Stevenson, R.J., 1992, Methods of determining the rheological properties of magmas at subliquidus temperatures: Journal of Volcanology and Geothermal Research, v. 53, p. 47–66.

Poli, S., and Schmidt, M.W., 2002, Petrology of subducted slabs: Annual Review of Earth and Planetary Sciences, v. 30, p. 207–235.

Ramberg, H., 1981, Gravity, deformation and geological application: New York, Academic Press, 452 p.

Ranalli, G., 1995, Rheology of the Earth (second edition): London, Chapman and Hall, 413 p.

Rosen, O.M., Zorin, Y.M., and Zayachkovsky, A.A., 1972, A find of a diamond linked with eclogites of the Precambrian Kokchetav massif: Dokladi Akademii Nauk SSSR, v. 203, p. 674–676 (in Russian).

Schmidt, M.W., and Poli, S., 1998, Experimentally based water budgets for dehydrating slabs and consequences for arc magma generation: Earth and Planetary Science Letters, v. 163, p. 361–379.

Sobolev, N.V., and Shatsky, V.S., 1990, Diamond inclusions in garnets from metamorphic rocks: A new environment for diamond formation: Nature, v. 343, p. 742–746.

Stern, R.J., 2002, Subduction zones: Review of Geophysics, v. 40, p. 3-1–3-38.

Stöckhert, B., Duyster, J., Trepmann, C., and Massonne, H.-J., 2001, Microdiamond daughter crystals precipitated from supercritical COH silicate fluids included in garnet, Erzgebirge, Germany: Geology, v. 29, p. 391–394.

Tamura, Y., 1994, Genesis of island arc magmas by mantle-derived bimodal magmatism: Evidence from the Shirahama Group, Japan: Journal of Petrology, v. 35, p. 619–645.

Tamura, Y., Tatsumi, Y., Zhao, D.P., Kido, Y., and Shukuno, H., 2002, Hot fingers in the mantle wedge: New insights into magma genesis in subduction zones: Earth and Planetary Science Letters, v. 197, p. 105–116.

Turcotte, D.L., and Schubert, G., 1982, Geodynamics: Application of continuum physics to geological problems: New York, John Wiley, 450 p.

Zhao, D.P., Mishra, O.P., and Sandra, R., 2002, Influence of fluid and magma on earthquakes: Seismological evidence: Physics of the Earth and Planetary Interiors, v. 132, p. 249–267.

Manuscript received 15 July 2003
Revised manuscript received 12 September 2003
Manuscript accepted 15 September 2003

Printed in USA